

# UW-CVGAN: UnderWater Image Enhancement with Capsules Vectors Quantization

Rita Pucci<sup>1\*</sup>, Christian Micheloni<sup>1</sup> and Niki Martinel<sup>1</sup>

<sup>1</sup>Department of computer science, University of Udine, via delle scienze, Udine, Italy.

\*Corresponding author(s). E-mail(s): [rita.pucci@uniud.it](mailto:rita.pucci@uniud.it);  
Contributing authors: [christian.micheloni@uniud.it](mailto:christian.micheloni@uniud.it);  
[niki.martinel@uniud.it](mailto:niki.martinel@uniud.it);

## Abstract

The degradation in the underwater images is due to wavelength-dependent light attenuation, scattering, and to the diversity of the water types in which they are captured. Deep neural networks take a step in this field, providing autonomous models able to achieve the enhancement of underwater images. We introduce Underwater Capsules Vectors GAN **UW-CVGAN** based on the discrete features quantization paradigm from **VQ-GAN** for this task. The proposed **UW-CVGAN** combines an encoding network, which compresses the image into its latent representation, with a decoding network, able to reconstruct the enhancement of the image from the only latent representation. In contrast with **VQ-GAN**, **UW-CVGAN** achieves the features quantization by exploiting the clusterization ability of capsules layer, making the model completely trainable and easier to manage. The model obtains enhanced underwater images with high quality and fine details. Moreover, the trained encoder is independent from the decoder giving the possibility to be embedded onto the collector as compressing algorithm to reduce the memory space required for the images, of factor **3**×. **UW-CVGAN** is validated with quantitative and qualitative analysis on benchmark datasets, and we present metrics results compared with the state of the art.

**Keywords:** Capsules Vectors, AutoEncoder, Underwater Images, Image Enhancement, GAN

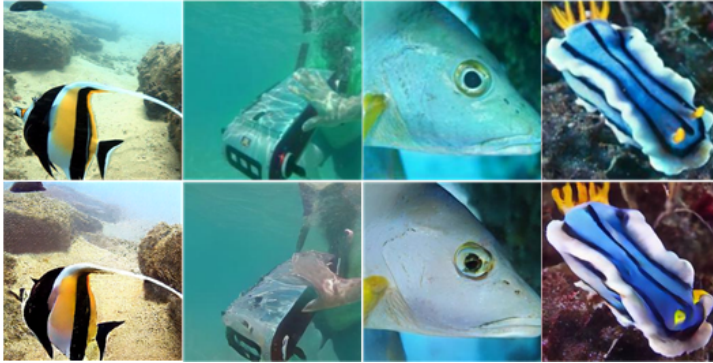


**Fig. 1** The first row shows the effects of water light refraction in underwater images. The second row shows the results of the proposed approach in removing the blurriness and cold tones due to the colours wavelength suppression.

## 1 Introduction

The Oceans cover most of the planet where we live and are as fascinating as harsh, complex, and dangerous for exploration. For these reasons, in recent years, the exploration and protection of the rich ecosystems result in sophisticated visual sensing systems used to capture information from the underwater world. These systems are often embedded in robots that are an attractive option because of their non-intrusive, passive, and energy-efficient nature. This underwater tools are efficient for monitoring the coral barrier reef [1], exploring the depth of the ocean [2], and analysing the seabed [3]. However, such methods are affected by the influence of water for light absorption and scattering that cause visible alteration in colours and definition of the images quality. As a consequence, underwater images often are hazy and show greenish or bluish tinged. For this reason, an intriguing challenge in computer vision is the enhancement task of these data.

Existing methods for underwater images enhancement include both traditional techniques (not based on machine learning algorithms) and deep learning-based techniques. The traditional techniques consist of non physical based methods, which adjust image pixel values to obtain visually neat images [4, 5], and physical based methods, which provide a precise restoration of the images requiring various complex underwater physical and optical factors [6, 7]. The former apply optical functions that are not generalised among different datasets, and the latter techniques need abundant data in order to extract the necessary factors [8]. In contrast, deep learning-based techniques are generalised over the data and have been recently applied for underwater image enhancement [8–15] with good results. These techniques automatically extract information from the images learning how to provide the enhancement of them.

We focus on deep learning-based techniques and in particular on the Generative Adversarial Networks (GAN) [16], that can automatically discover and

learn the regularities or patterns in input data so that the model can be used to generate and reconstruct samples [17]. In the field of enhancement of underwater images, the main disadvantage by using GAN is that the category attribute of the image cannot be controlled, resulting in blurry images. Works at SOTA, mitigate this problem by using conditional information. In [9], authors perform a fast enhancement of underwater images by adding to the input random noise and associating to the loss function additional aspects rather than just the adversarial one. Other works [8, 10, 12] are based on a cycle-consistent adversarial network (CycleGAN) [13] that demonstrate to obtain good results. They require a multi-term objective function for the generator loss, to correct colour casts effectively, and to improve image quality. In [14], the authors provide a simultaneous enhancement and super-resolution of the underwater image by a fully convolutional encoder-decoder architecture. In contrast with these works, we want to avoid the conditioning of the model by using only the underwater images without additional information. This reduces the amount of data that has to be set for the enhancement process.

Further works avoid the conditioning by using U-Net shape to keep spatial information through the reconstructive process [9, 11, 15]. In [15], the authors proposed a multiscale dense block to concatenate the features among the features extraction and features reconstruction phases. In [9, 11], the authors input only the underwater image and use a U-Net based structure to enhance it using skip connections to conserve the spatial information among the reconstruction layers. In fact, models based on U-Net structure create a strong connection between the features extraction and the image reconstruction phases, that do not give the possibility to separate the two phases and to obtain a compression algorithm. We think that the compression of the images avoid wasting memory space for useless information and for this idea, we propose a model that provides the compression of the images to their features representations and that is able to reconstruct the enhanced image from them.

For such a model, we consider the Variational AutoEncoder (VAE) family models. In fact, the VAE consists of encoder-decoder networks which learn to represent the input data in a latent representation and reconstruct them in the output. The latent representation is extracted through encoder by the latent space, which describes the probability distribution of the data learned by the model in the training phase. It is worth noting that in VAE, the encoder and the decoder are two separated networks.

The Variational Quantized AutoEncoderVQ-VAE [18] encodes features as discrete latent variables by a quantized latent space and offers a direct control over the information content of the learned representation. Even if the quantization provides a good property of features separation [19, 20], a discrete latent representation is not differentiable, making the training phase challenging. There exist strategies to circumvent the differentiability problem, such as optimise the mean output of discrete random units [21], altering the training dynamics methods [22], or applying a straight-through gradient estimator, which copies the gradients from the decoder to the encoder [18, 23]. We think

that the idea of quantization of the latent space used for features representation is a good strategy to obtain a model able to reconstruct high quality images and that can be applied to extract the fundamental features from underwater images leaving the noise of water behind. However the non differentiability represents a limit to the possibilities of the model, and we propose a model that takes into consideration this aspect.

We propose **CV-GAN**, a generative VAE model based on Capsules Vectors [24–27] that exploits the quantization idea by maintaining the model completely differentiable. Works in image analysis [28, 29] exploit capsules for colours reconstruction and image classification and demonstrate the capsules’ clusterization ability.

**CV-GAN** is a tradeoff between a fully differentiable VAE and a discrete latent representation. Our model provides a learned continuous latent space where the features quantization is implemented by capsules layer. This layer represents each input image as the clustered probability distribution of features which represent the entities in the image. In particular, we replace the discrete quantized vectors proposed in **VQ-VAE** with the capsules vectors by replacing the code-book used in **VQ-VAE** with the capsule layer. The clusterization of these vectors is obtained by the routing-by-agreement (**RbA**) [24]. With **RbA**, the layer learns a dynamic representation of the features clustering them into the capsules vectors. We demonstrate that the capsules vectors is the latent representation of the image and this representation can be used for the reconstruction of the enhancement of the image.

In contrast to [9, 11], our model needs only the latent compression of the image for the reconstruction of the enhancement of the image, and the encoder network can be used as compression algorithm for the image collected. The compression obtained is of  $3\times$  of the original dimension of the images; we identify [14] which provide good metric results but with a lower compresses of the original dimension. The use of VAE models for the enhancement task is presented in [30, 31], with not generative models conditioned by the simulation of the effects of optical factors.

The application of **CV-GAN** model for the task of underwater images enhancement is here after denoted by **UW-CVGAN**. **UW-CVGAN** outperforms the results on metrics obtained with **VQ-GAN** in the proposed task and both following the training phase described in Sec. 4.1. Moreover, our model is differentiable, still maintaining the features quantization characteristic. We evaluate **UW-CVGAN** on benchmarks datasets and we compare the results with GAN models proposed for enhancement of underwater images.

The main contributions of this paper are summarised as follows.:

- we propose a novel VAE model based on capsules layer named **UW-CVGAN** which exploits the **RbA** procedure as clusterization paradigm for the enhancement of underwater images;
- we demonstrate that the new model is completely differentiable, still implementing the quantization of the latent space;





**Fig. 2** Image samples shot in underwater environment. These samples show some of the typical problem with underwater images, from the left: low edge definition, blueish colours, greenish colours, blurriness. These images are from EUVP,UFO120,HICRD,UIEB datasets.

- we demonstrate that the encoder provides a latent representation of the image that is sufficient to the decoder to reconstructs the image enhanced in quality;
- the separated encoder-decoder networks in UW-CVGAN give the possibility to embed the encoder network into the collector to compress the images by a factor of  $3\times$  storing only the latent representation.

This is the first attempt of applying capsules to learn a latent space and, in particular, for image enhancement. We think that the clusterization offered by the capsules layer is a valid candidate for the latent space implementation and that the results obtained in underwater image enhancement demonstrate the ability of the model in features extraction. A detailed discussion will be presented in Sec. 3.2.

## 2 Background

### 2.1 Underwater images

Underwater images are characterised by a whole range of light distortions due to the water absorption of light waves. The colours and the edges' perception change with depth, illumination, and turbidity of water making the image appear completely different. The low definition of edges, the distortion of colours in a blueish or greenish colourisation, and the distortion of light make the identification of subjects in the image difficult. In Fig. 2, we show some samples of the high variability in visual scenes that may occur in underwater environments. It is necessary for the vision-based algorithms in this field, to reach a good generalisation in order to work within this range of distortions. Some physics-based models in this field consider the Jaffe-McGlamery model [32, 33] which is able to describe the underwater image degradation by defining the distorted images as follows:

$$I(x) = J(x)t(x) + \alpha(1 - t(x)) \quad (1)$$

where  $I(x)$  denotes the degraded image, and  $J(x)$  is the clear image. The parameter  $\alpha$  is the global atmospheric light and it indicates the intensity of ambient light, and the  $t(x) \in [0, 1]$  is the transmission map matrix which denotes the percentage of the scene radiance reaching the camera. It is defined

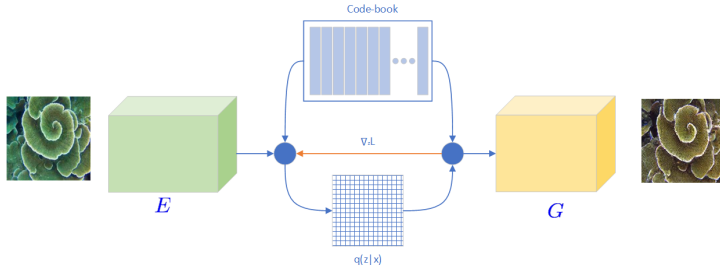


**Fig. 3** The VQ-VAE [18, 23] model. The output of the encoder  $z^{\mathbf{e}(\mathbf{X})}$  is quantized based on a code-book randomly initialised. The application of a discrete quantization makes the connections with  $q(\cdot)$  not differentiable. By the straight through estimator, the gradient  $\nabla_z L$  will push the encoder to change its output without taking into consideration the quantization step.

as:

$$t(x) = e^{-\nu d(x)} \quad (2)$$

where  $\nu$  is the atmospheric attenuation coefficient and  $d(x)$  is the distance of the object to camera. Even if this model is straightly related to the real nature of the underwater distortions in the images, the application of such a model to represent the image is a challenging task due to the high parametrization which requires estimating  $\alpha$ ,  $\nu$  and  $d(x)$  in different underwater environments. It is to consider that the disparity of the underwater conditions present in nature is often much more complicated to represent than the possibilities offered by this model. Deep neural networks demonstrate to be a valid alternative to the physics-based models. These models are trained to extract representative features for images without any environmental information, providing good results with a wide range of underwater scenes.

## 2.2 Variational Auto-Encoder (VAE)

VAE is a deep convolutional neural network algorithm introduced in [31], it belongs to the families of probabilistic graphical models and variational Bayesian methods. This model consists of an encoder ( $E$ ) and a decoder ( $G$ ) networks. The encoder network parameterises a posterior distribution  $q(z|\mathbf{X})$  of latent random variables  $z$  given the input data  $\mathbf{X}$ , and a prior distribution  $p(z)$ . The encoder must learn an efficient compression of the data into this lower-dimensional space, the latent space. The decoder network receives the representation  $z$  and outputs the probability distribution of data, so it is denoted by a distribution  $p(\mathbf{X}|z)$ . The posteriors and priors in VAE are assumed to be normally distributed with diagonal covariance.

## 2.3 Vector Quantized Variational Auto-Encoders (VQ-VAE)

An interesting architecture based on VAE is the VQ-VAE model [18]. These models propose a new latent space where a quantization function is used to represent the latent vectors. The latent space is defined as  $\mathbf{e} \in \mathbb{R}^{K \times M}$  where  $K$  is

the size of the discrete latent space (i.e.,  $K$ -way categories for the quantization), and  $M$  is the dimensionality of each latent vector  $\mathbf{e}^i \in \mathbb{R}^M$ ,  $i \in 1, 2, \dots, K$  that compose the code-book, as shown in Fig. 3. The input to  $G$  is the corresponding embedding vector  $\mathbf{e}^k$ .

These models are regular autoencoders with a particular non-linearity that maps the latents to 1-of- $K$  code-book. The complete set of parameters for the model is the union of parameters of  $E$ ,  $G$ , and the embedding space  $\mathbf{e}$ . In contrast with  $E$  and  $G$  parameters, the embedding space is discrete and is not trainable with the canonical strategy of backpropagation of gradients. This characteristic makes the latent space on one side easier to manage and on the other side difficult to train.

## 2.4 Capsules Layer

A capsule is a set of neurons which capture the presence of an entity in an image [24] by clustering the features extracted. The capsules collectively produce an activation vector with one element from each neuron to hold that neuron’s instantiation value. In a hierarchical structure of capsules layers, the activation vector of each capsule of the higher layer makes predictions for the parent capsules. Capsules layers are trained by the **RbA** mechanism. This mechanism compares the higher layer prediction with the activation vector of the parents-capsules. The activation vectors which match are clusterised to provide the final vector that represents the probability of the entities to be present. In Sec. 3.2 we demonstrate that the capsules and **RbA** are promising ideas for a dynamic clusterization of the features in **VQ-VAE**. Such a solution is still not explored at the SOTA in **VAE** and we think that can be a good trade-off between a continuous latent space and the discrete latent space of **VQ-VAE** made by a fixed code-book. We propose a capsules layer to cluster the representative variables to compute the distribution of the features as a replacement for the quantization. This makes the training procedure completely differentiable while maintaining the clustering idea of the feature representation.

## 2.5 Generative Adversarial Network

The Generative Adversarial Network [16] is a framework for generative modelling of data through learning a transformation from points belonging to a prior distribution ( $z \sim p_z$ ) to points from a data distribution ( $\mathbf{X} \sim p_{data}$ ). It consists of two models that play an adversarial game: a generator  $G$  and a discriminator  $D$ . While  $G$  attempts to learn the aforementioned transformation  $G(z)$ ,  $D$  acts as a critic  $D(\cdot)$  determining whether the sample provided to it is from the generator’s output distribution ( $G(z) \sim p_G$ ) or from the data distribution ( $\mathbf{X} \sim p_{data}$ ), thus giving a scalar output ( $y \in \{0, 1\}$ ). The generator wants to fool the discriminator by generating samples that resemble those from the data distribution, while the discriminator wants to accurately distinguish between real and generated data. The two models are neural networks

and they play an adversarial game with the objective:

$$\min_G \max_D V(D, G) = E_{\mathbf{X} \sim p_{data}(\mathbf{X})} [\log D(\mathbf{X})] + E_{z \sim p_z(z)} [\log(1 - D(G(z)))] \quad (3)$$

## 3 Methods

### 3.1 Capsules layer architecture

Let  $\mathbf{u}_i \in \mathbb{R}^{d_u}$  be an output of a capsule  $i$  at layer  $L$ , and  $j$  the index at layer  $L + 1$ . The affine transformation of  $\mathbf{u}_i$  is calculated as:

$$\hat{\mathbf{u}}_{i|j} = \mathbf{W}_{ij} \mathbf{u}_i \quad (4)$$

where the  $\mathbf{W}_{ij} \in \mathbb{R}^{d_u \times d_a}$  is a weighted matrix that given an activation vector  $\mathbf{u}_i$  provides a prediction vector  $\hat{\mathbf{u}}_{i|j}$ . Not all the capsules at layer  $L$  are similarly affecting the capsules at layer  $L + 1$ . The procedure identifies the coupling coefficients  $c_{ij}$  that express the importance of capsule  $i$  at lower layer for capsule  $j$  at a higher layer. The  $c_{ij}$  are computed by applying the soft-max function over  $b_{ij}$ :

$$c_{ij} = \frac{\exp(b_{ij})}{\sum_k \exp(b_{ik})} \quad (5)$$

where  $b_{ij}$  is log probability of capsule  $i$  being coupled with capsule  $j$ . The  $b_{ij}$  variable is initialised at 0, then it is updated  $\alpha$  times, at each iteration of the RbA procedure. Then, the input vector of capsule  $j$  is computed as the weighted sum of the probability vectors at capsule  $i$  multiplied by the coupling coefficient:

$$\mathbf{s}_j = \sum_i c_{ij} \hat{\mathbf{u}}_{j|i} \quad (6)$$

By having the input vector of capsule  $j$  at higher layer, the clustering procedure is implemented by computing the agreement among capsules, as shown in Fig. 4. The output vectors of the capsules layer represent the probability of an object of being present in the given input or not. These vectors can exceed value one, depending on the output, so to make the output vector represents a probability, a non linear squashing function is used to restrict the vector length to one, where  $\mathbf{s}_j$  is input to capsule  $j$  and  $\mathbf{v}_j$  is the output.

$$\mathbf{v}_j = \frac{\|\mathbf{s}_j\|^2}{1 + \|\mathbf{s}_j\|^2} \frac{\mathbf{s}_j}{\|\mathbf{s}_j\|} \quad (7)$$

Finally  $b_{ij}$  are updated by computing the inner product of  $\mathbf{v}_j$  and  $\hat{\mathbf{u}}_{j|i}$ . If two vectors agree, the product would be larger leading to longer vector length. We summarise the RbA in Algorithm 1.

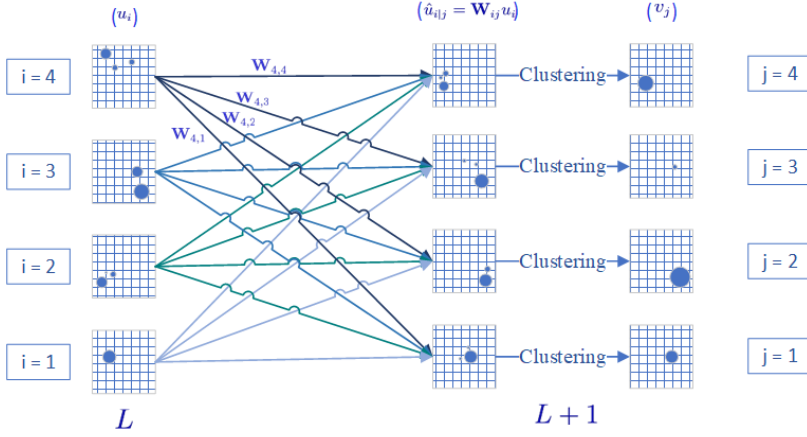


**Fig. 4** Visual representation of the RbA paradigm: the output of the capsules at layer  $L$ ,  $\mathbf{u}_i$ , is forwarded to the capsules at the upper layer  $L + 1$ . An affine transformation is applied to obtain  $\hat{\mathbf{u}}_i$ . Then the features are clustered in  $\mathbf{v}_j$  based on the agreement among capsules.

---

**Algorithm 1** RbA algorithm [24]

---

**Require:**  $\mathbf{u}_i \in \mathbb{R}^{d_u}$

**Ensure:**  $\hat{\mathbf{u}}_{i|j} = \mathbf{W}_{ij}\mathbf{u}_i$

**for** all capsule  $i \in [0, \beta]$  in layer  $L$  **do**

**for** all capsule  $j \in [0, \beta]$  in layer  $L+1$  **do**

$b_{ij} \leftarrow 0$

**for**  $\alpha$  iteration of routing **do**

$$c_{ij} = \frac{\exp(b_{ij})}{\sum_k \exp(b_{ik})} \quad (\text{Eq. 5})$$

$$\mathbf{s}_j = \sum_i c_{ij} \hat{\mathbf{u}}_{j|i} \quad (\text{Eq. 6})$$

$$\mathbf{v}_j = \frac{\|\mathbf{s}_j\|^2}{1 + \|\mathbf{s}_j\|^2} \frac{\mathbf{s}_j}{\|\mathbf{s}_j\|} \quad (\text{Eq. 7})$$

$$b_{ij} \leftarrow b_{ij} + \mathbf{v}_j \hat{\mathbf{u}}_{j|i}$$

**end for**

**end for**

**end for**

---

### 3.2 Clustering of representative learning

Clustering implies partitioning data into meaningful groups such that items are similar within each group and dissimilar across different groups. We observe that capsules with RbA implement a clusterization procedure. In Eq. 5, the coupling coefficients  $c_{ij}$  is large for  $(i, j)$  if capsule  $i \in L$  is meaningful for capsule  $j \in L + 1$ , and small otherwise. Such that  $\hat{\mathbf{u}}_{i|j}$  is similar to others  $\hat{\mathbf{u}}_{k|j}$ , with  $k \neq i$ , if both depict meaningful information for capsule  $j \in L + 1$ .

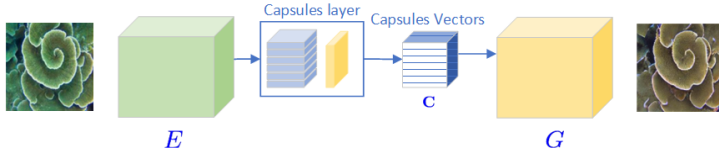


**Fig. 5** The proposed CV-GAN: VAE with newly proposed a latent space obtained by the capsules layer which implement the clustering of features.

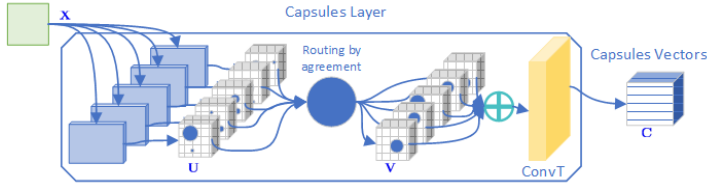


**Fig. 6** Proposed CL of CV-GAN: it consists of a capsules layer and a convolution transpose layer. The capsules extract  $\mathbf{U}$  features which are clusterised by the RbA procedure, to obtain  $\mathbf{V}$ . We aggregate the matrices and upsample by the convolutional transposed layer.

In Fig 4,  $\hat{\mathbf{u}}_{ij}$ , depicted by blue circles, denote the agreements at layer  $L$ . These agreements are empowered by  $c_{ij}$  in the clusterization phase, shown with the "Clustering" arrow, to obtain  $\mathbf{v}_j$ . By squashing  $\mathbf{s}_j$ , we interpret  $\mathbf{v}_j$  as the probability that capsule  $i$  is grouped to cluster  $j$ . The  $\mathbf{v}_j$  for all the  $j$  in  $L$ , represents the capsules vectors for the input. We think that the clusterization obtained by the capsules layer is a tradeoff between the random latent variables learned in VAE and the discrete latent representation obtained with VQ-VAE. In contrast with VQ-VAE, in CV-GAN we have the differentiability of the entire structure with the RbA procedure and similar to the VQ-VAE, we introduce the clusterization property of the latent variables which reduces the latent space generated by the model.

### 3.3 CV-GAN architecture

In Fig. 5, we present the new model CV-GAN. It is a convolutional model consisting of an encoder  $E$ , a new latent space based on capsules layer  $CL$ , and a decoder  $G$ , such that they learn to represent images with latent variables from a learned representation made by capsules vectors. We follow the implementation proposed in VQ-GAN for the  $E$  and  $G$  networks. The  $E$  network consists of six blocks with  $\{\text{ResNet} - \text{Attention} - \text{Convolution}\}$ .  $E$  receives as input an image  $\mathbf{Y} \in \mathbb{R}^{c_{\text{input}} \times h_{\text{input}} \times w_{\text{input}}}$  and extracts an hidden/latent representation  $\mathbf{X} \in \mathbb{R}^{c_z \times h_z \times w_z}$  defined in the latent space  $z$ .  $z(\mathbf{X})$  is the input of  $CL$ .  $CL$  has  $\beta$  capsules implemented with convolutional layers that compute  $\beta$  different views,  $\mathbf{U}$ , of the input  $\mathbf{X}$ , Fig. 6. The  $\mathbf{U} \in \mathbb{R}^{\beta \times d_u \times h \times w}$  consists of the activity vectors, each of which with  $d_u$  digits. They are collectively produced by neurons in capsules at layer  $L$ . Each view in  $\mathbf{U}$  consists of  $h \times w$  vectors. With their length and orientation, these vectors represent the presence and properties of entities identified in the image. Following the RbA procedure described

in Sec. 3.1, the capsules layer is able to cluster the extracted  $\mathbf{U}$  features, and to remove the unclustered ones. In particular, the **RbA** maintains the features depicted as present by the agreement among the capsules. The *CL* provides  $\mathbf{V} \in \mathbb{R}^{\beta \times d_a \times h \times w}$ , where  $d_a$  is the number of digits of each vector obtained. We aggregate the features in  $\mathbf{V}$  by computing the  $L_1$  norm of each vector, flattening  $\mathbf{V}$  to  $\mathbb{R}^{\beta \times h \times w}$ . Finally, a convolutional layer maps the flattened  $\mathbf{V}$  into  $\mathbf{C} \in \mathbb{R}^{c_C \times h_C \times w_C}$  that is the input of the decoder network.

The decoder network  $G$  is composed by six blocks, each of which is composed of  $\{\text{ResNet} - \text{Attention} - \text{Upsampling}\}$ . This network reconstructs the image from  $\mathbf{C}$  to generate an output image  $\hat{\mathbf{Y}} \in \mathbb{R}^{c_{input} \times h_{input} \times w_{input}}$  where the noise due to the underwater situation is removed.

### 3.4 Loss Function

The proposed **CV-GAN** is trained to compress the essential features of the image in the capsules vectors at the latent space. We want that these features are the information about the subjects present in the image and that the model leaves behind the noise information. With this intent, we consider paired training samples for high-quality enhancement and we train the pretrained **CV-GAN** to reconstruct the input image as it is. The model is then fine-tuned for the denoising task. We observe that the pretraining of the model let the model build progressively the ability of reconstruction and denoise of the images .

#### 3.4.1 Adversarial loss

We train the model with the adversarial training procedure with a patch-based discriminator  $D$  [34] that aims to differentiate between real and reconstructed images. The generator  $G$  is implemented with the proposed model and it is conditioned on an underwater image  $\mathbf{I}$  given as input to the model. We want the model to produce an image to try and fool  $D$ . Meanwhile,  $D$  is trained to distinguish between the original not distorted images and the images generated by  $G$ . We follow the original formulation of  $\mathcal{L}_{GAN}$  proposed in [23].

$$\mathcal{L}_{GAN}(E, G, CL, D) = \lambda [\log D(\mathbf{Y}) + \log(1 - D(\hat{\mathbf{Y}}))] \quad (8)$$

The  $\hat{\mathbf{Y}}$  denotes the output obtained by  $G$  while  $\mathbf{Y}$  is the ground-truth image. The contribution of the  $\mathcal{L}_{GAN}$  is controlled by factor  $\lambda$  that is an adaptive weight computed according to:

$$\lambda = \frac{\nabla_{G_L}[\mathcal{L}_{rec}]}{\nabla_{G_L}[\mathcal{L}_{GAN}] + \delta} \quad (9)$$

where  $\mathcal{L}_{rec} = \|\mathbf{Y} - \hat{\mathbf{Y}}\|^2$  is the perceptual reconstruction loss [35],  $\nabla_{G_L}[\cdot]$  is the gradient of its input at the last layer  $L$  of the decoder, and  $\delta$  is used for numerical stability [23].



### 3.4.2 Gradient difference loss

We observe that generative models produce blurry images while reconstructing the underwater image. For this reason, in fine-tuning we add a sharpener factor to the loss function. This sharpener factor consists of directly penalise the differences of image gradient predictions in the generative loss function. We apply the Gradient Difference Loss (GDL) function [36]. This function between the ground truth image  $\mathbf{Y}$ , and the prediction  $\hat{\mathbf{Y}}$  is given by:

$$\mathcal{L}_{GDL}(\mathbf{Y}, \hat{\mathbf{Y}}) = \sum_{ij} \|\mathbf{Y}_{ij} - \mathbf{Y}_{i-1j}\| - \|\hat{\mathbf{Y}}_{ij} - \hat{\mathbf{Y}}_{i-1j}\|^\gamma + \|\mathbf{Y}_{ij-1} - \mathbf{Y}_{ij}\| - \|\hat{\mathbf{Y}}_{ij-1} - \hat{\mathbf{Y}}_{ij}\|^\gamma \quad (10)$$

where  $\gamma$  is an integer greater or equal to 1, and  $|\cdot|$  denotes the absolute value function. The GDL penalises gradient differences between the reconstructed and the real output. In this work, the image gradient is obtained by considering the neighbour pixel intensities differences, rather than adopting a more sophisticated norm on a larger neighbourhood, to keep the training time low.

### 3.4.3 Combined loss

In our experiments, we apply the  $\mathcal{L}_{CV-GAN}$  for the network CV-GAN, during pretraining. It is defined as:

$$\mathcal{L}_{CV-GAN} = \mathcal{L}_{rec} + \mathcal{L}_{GAN}(E, G, CL, D) \quad (11)$$

The function applied for UW-CVGAN obtained by "Underwater images training phase" considers the combination with the  $\mathcal{L}_{GDL}$  to promote a sharper reconstruction. The contribution of the GDL function is considered in the ablation study at Sec. 4.4. In this phase we define  $\mathcal{L}_{UW-CVGAN}$  as:

$$\mathcal{L}_{UW-CVGAN} = \mathcal{L}_{rec} + \mathcal{L}_{GAN}(E, G, CL, D) + \mathcal{L}_{GDL} \quad (12)$$

## 4 Results

### 4.1 Dataset

We consider CV-GAN pretrained on ImageNet dataset and we fine-tune the model for the underwater images task. Following [23], we consider the ImageNet dataset [37] and we pretrain CV-GAN for image reconstruction on the training split suggested for the ImageNet dataset consisting of 1.3M images (with no labels). The input images are resized to  $256 \times 256$ . We identify the model at this stage with the name CV-GAN.

#### *Training phase:*

The CV-GAN pretrained on ImageNet is fine-tuned for the image denoising task on the training split suggested for UFO120 dataset. The UFO120 dataset [14] comprises 1500 samples shot underwater with no labels. Each sample consists

of a noisy and denoised images pair. The noisy image is shot underwater and it shows water distortion, while the denoised image does not have the water distortion. We identify the CV-GAN fine-tuned for underwater images with the name UW-CVGAN.

### ***Validation phase:***

We evaluate the model over four benchmarks: Enhancing Underwater Visual Perception (EUVP), Heron Island Coral Reef Dataset (HICRD), Underwater Image Enhancement Benchmark (UIEB), and Underwater Image Super-Resolution (USR248). The dataset EUVP [9] consists of separate sets of paired and unpaired image samples of poor and good perceptual quality to facilitate supervised training of underwater image enhancement models. We take into consideration the validation split of paired images, which consists of 1970 images. The HICRD [38] is a set of images shot to the coral reef at deep sea with 300 pairs of images. The UIEB [39] includes 877 images, which involve richer underwater scenes (lighting conditions, water types, and target categories) and better visual quality reference images than the existing ones. Finally, the USR248 [14] contains 248 samples of underwater images. The latter two datasets consist only of the underwater images with not denoised pairs.

## **4.2 Implementation details**

The input the UW-CVGAN is  $\mathbf{Y} \in \mathbb{R}^{3 \times 256 \times 256}$ . The network  $E$  outputs  $z(\mathbf{X}) \in (R)^{256 \times 16 \times 16}$ , which is the input of  $CL$ . This consists of  $\beta = 32$  capsules and outputs  $\mathbf{U} \in \mathbb{R}^{32 \times 16 \times 9 \times 9}$  through convolutional layers. The  $[32 \times 9 \times 9]$  tensors, which are extracted by the capsules, describe the different points of view of the capsules and each vector has  $d_u = 16$  digits. In RbA, we set  $\alpha = 3$  for the  $c_{i,j}$  loop update. The output of RbA is  $\mathbf{V} \in \mathbb{R}^{32 \times 64 \times 9 \times 9}$ , where each vector obtained by clusterisation has  $d_a = 64$  digits. The transposed convolution layer in the capsules layer outputs  $\mathbf{C} \in \mathbb{R}^{256 \times 16 \times 16}$ .

Finally,  $G$  decodes  $\mathbf{C}$  to generate the output matrix  $\hat{\mathbf{Y}} \in \mathbb{R}^{3 \times 256 \times 256}$ . The UW-CVGAN models  $X = 3 \times 256 \times 256$  images by compressing them to  $z = 256 \times 16 \times 16$  latent space via the capsules layer  $p(\mathbf{X}|z)$ . In particular, the compression factor obtained with the latent representation  $z$  is:

$$\frac{3 \times 256 \times 256}{256 \times 16 \times 16} = 3 \quad (13)$$

We consider the batch size set to 6. The CV-GAN is pretrained to reconstruct the input image  $\mathbf{Y}$  while we train the UW-CVGAN to reconstruct the denoised input denoted with  $\mathbf{Y}_d \in \mathbb{R}^{3 \times 256 \times 256}$ . For the experimentation, the proposed models, CV-GAN and UW-CVGAN, is trained respectively for 25 and 500 epochs. Finally, we set  $\delta = 10^{-6}$  in Eq. 9, as suggested in [23], and  $\gamma = 1$  in Eq. 10.

### 4.3 Metrics

The UW-CVGAN model is evaluated qualitatively, by considering the visual presentation of the reconstructed and enhanced images, and quantitatively, by comparing our metrics results with the SOTA. In particular, we consider the Inception Score (IS) [40], the Peak Signal-to-Noise Ratio (PSNR) [41], the Underwater Color Image Quality Evaluation Metric (UCIQE) [42], and the Underwater Image Quality Measure (UIQM) [43]. PSNR, IS metrics analyse the reconstruction quality obtained by the model, while UCIQE and UIQM are specific for the underwater images enhancement. The IS evaluates the quality of the image obtained by generative models by applying an Inception v3 Network pretrained on ImageNet. This quality is calculated as a statistic of the network’s outputs when applied to generated images. We apply IS according to project [44]. The PSNR evaluates the quality between the original and a reconstructed image. The higher the PSNR, the better the quality of the reconstructed image. Even if UW-CVGAN is a generative model, we consider the PSNR a valid metric to evaluate the reconstruction ability of the model. The UCIQE is a linear combination of chroma, saturation, and contrast. It is proposed to quantify the non-uniform colour cast, blurring, and low-contrast that characterised underwater engineering and monitoring images. Finally, the UIQM comprises three underwater image attribute measures: the underwater image colorfulness measure (UICM), the underwater image sharpness measure (UISM), and the underwater image contrast measure (UIConM). Each attribute is used to assess each singular aspect of the underwater image degradation. Therefore, the UIQM is the combination of the three, as  $UIQM = c_1UICM * c_2UISM * c_3UIConM$  where the colorfulness, sharpness, and contrast measures are linearly combined. We set the three parameters  $c_1$ ,  $c_2$ , and  $c_3$  to 0.0282, 0.2953, and 3.5753 according to the paper [43].

### 4.4 Ablation study

The ablation study aims to reveal the effect of two main characteristics of the proposed model: 1) the impact of each component applied in the loss function; 2) the comparison between the usage of the Capsules vectors in UW-CVGAN and the discrete quantization, VQ-GAN. For this second point, the two models are trained under the same condition and with the same dataset. All the models presented in the ablation study are pretrained on ImageNet and fine-tuned on UFO120, as specified in Sec. 4.1. Fig. 7 shows the reconstruction of images from EUVP and UIEB datasets.

In the samples shown in Fig. 7, the first row presents the input image from the original dataset. We compare results obtained with and without the application of the  $\mathcal{L}_{GDL}$  component. The second row shows the reconstruction obtained with UW-CVGAN where the  $\mathcal{L}_{GDL}$  component is not added to the  $\mathcal{L}_{UW-CVGAN}$ . In this case, the  $\mathcal{L}_{UW-CVGAN}$  corresponds to Eq. 11. We compare these results with the third row images, where the  $\mathcal{L}_{GDL}$  is present in  $\mathcal{L}_{UW-CVGAN}$



**Fig. 7** Ablation analysis: First row shows the input images. In the second row, the results of UW-CVGAN w/o  $\mathcal{L}_{GDL}$ , and in the third row of UW-CVGAN with  $\mathcal{L}_{GDL}$ . Last row, we present results obtained with the VQ-GAN model, that is the direct competitor with the UW-CVGAN. The samples are from the EUVP test split dataset and UIEB dataset.

defined by Eq. 12. We observe that the quality of the images obtained with  $\mathcal{L}_{UW-CVGAN}$  = Eq. 12 is higher, and the contours appear well defined. This observation is supported by the quantitative results presented in Tab. 1, which summarises the metric results obtained with the four benchmark datasets proposed for validation. The results obtained with UW-CVGAN are higher in almost all considered metrics compared to the results provided by UW-CVGAN w/o GDL. Based on this observation, we demonstrate that the application of the  $\mathcal{L}_{GDL}$  provides fundamental information for the reconstruction of the image reaching high-quality results. The PSNR, metric is not available for UIEB and USR248 datasets because the ground truth is not available at SOTA.

We now compare the results obtained with UW-CVGAN (third row) and results with VQ-GAN (fourth row). In Fig. 7 and Tab. 1, we observe that the application of capsules layer in the UW-CVGAN, provides a visible improvement in the quality of the reconstruction compared with the reconstruction obtained with VQ-GAN. In the third row (from the top), the images appear to have higher quality with well-defined edges of the entities represented compared to the images at the fourth row (from the top). This observation is visible also in metrics (Tab. 1), where UW-CVGAN achieves better results in almost all the datasets considered.

**Table 1** Ablation Study Metrics: We summarise the results obtained with the UCIQE, UIQM, PSNR, and IS metrics. The table compares different implementations of the UW-CVGAN trained with/without  $\mathcal{L}_{GDL}$ , and the VQ-GAN.

dataset	model	UCIQE $\uparrow$	UIQM $\uparrow$	PSNR $\uparrow$	IS $\uparrow$
EUVP	UW-CVGAN	<b>6.47</b>	<b>2.91</b>	<b>29.11</b>	$4.39 \pm 0.5$
	UW-CVGAN w/o GDL	6.32	2.50	28.93	<b>5.02</b> $\pm 0.1$
	VQGAN	6.31	2.39	28.90	$4.82 \pm 0.2$
HICRD	UW-CVGAN	<b>3.59</b>	<b>2.15</b>	<b>28.11</b>	$1.87 \pm 0.1$
	UW-CVGAN w/o GDL	3.40	2.05	28.09	<b>1.96</b> $\pm 0.1$
	VQGAN	3.32	1.95	28.10	$1.93 \pm 0.1$
UIEB	UW-CVGAN	<b>5.46</b>	<b>3.41</b>	-	<b>3.73</b> $\pm 0.3$
	UW-CVGAN w/o GDL	5.26	2.64	-	$3.60 \pm 0.4$
	VQGAN	5.34	2.38	-	$3.38 \pm 0.4$
USR248	UW-CVGAN	6.46	<b>2.43</b>	-	$4.72 \pm 0.6$
	UW-CVGAN w/o GDL	6.21	2.03	-	<b>5.03</b> $\pm 0.8$
	VQGAN	<b>6.53</b>	1.90	-	$4.93 \pm 0.5$

## 4.5 Results Comparison

We consider the Deep Ssr [14], Funie gan [9], Ugan and Ugan-p [11] works to provide a qualitative and quantitative comparison evaluation. The evaluation presented is performed on the EUVP dataset, commonly used for evaluation by all the works considered for comparison. In Fig. 8, we qualitatively compare the reconstructed images provided by UW-CVGAN (second column) and by the others works(third-sixth columns). We observe that the images provided by UW-CVGAN have neat images and overall better quality than the SOTA. In all the images, the subjects are reconstructed with a bright colourisation and a wealth of details.

To support this observation, in Fig. 9, we show two samples from EUVP dataset focusing on details in the images. The yellow square identifies the area of the images that is the object of the zoom. In the first row, we present a blue and white sea slug body. In the first column, the reconstructed body of the animal has a high quality definition of details and the colours appear to be smooth and bright. On the contrary, the reconstructions obtained with SOTA methods have low in quality. In the second row, we zoom on the detail of the fin of the fish. We observe results similar to the slug: the reconstruction obtained with our model outperforms other methods for image quality and the definition of details. It is worth noting that these results demonstrate how the UW-CVGAN is able to reconstruct the enhanced input image by decoding only the latent variables. Tab. 2 shows results obtain on the EUVP dataset. We compare UW-CVGAN with the models at SOTA over the metrics considered for evaluation. We observe that our proposed method achieves results that are in line with SOTA in all the metrics. The last two columns in Tab. 2 denote the number of parameters per image/latent representation and the byte required for storing them. We observe that UW-CVGAN can store the only latent representation which





**Fig. 8** Comparison of the reconstructed images: The first column shows the input images provided to the models for the denoising task. We compare our results with EUVP dataset (second column from the left, in the orange rectangle), with results obtained with models at the state of the art Deep Ssr [14], Funie gan [9], Ugan and Ugan-p [11]. Last column is the ground truth of the denoised images.

consists of less parameters than the original input image. In Deep Ssr [14], the dimension of the encoded image requires  $1.1MB$  required while with UW-CVGAN it is less than  $300KB$ . In contrast with Funie gan [9], Ugan and Ugan-p [11],  $E$  and  $G$  in UW-CVGAN are not entangled with skip connection resulting in the possibility of storing only the encoded image ( $256 \times 16 \times 16$ ).

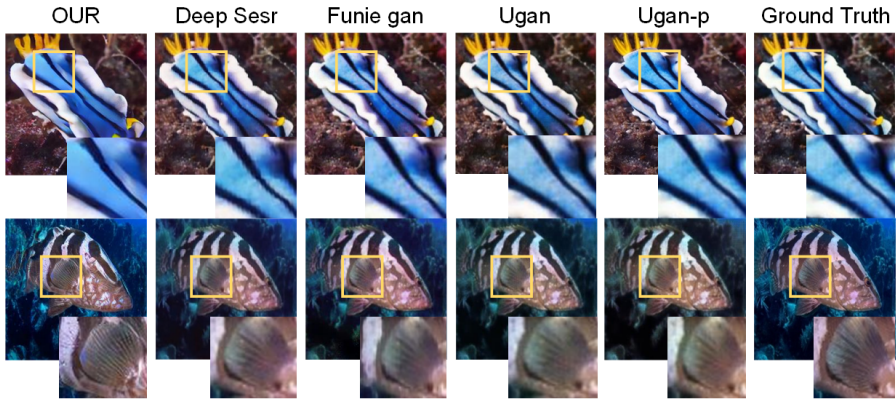


**Fig. 9** Focus of reconstruction quality of images: The first column shows the denoising and reconstruction of images from EUVP dataset with proposed *UW-CVGAN* (second column from the left). We compare our model with results obtained with models Deep Ssr [14], Funie gan [9], Ugan and Ugan-p [11]. Last column is the ground truth of the denoised images.

**Table 2** Results Comparison Metrics: We summarise the results obtained on UCIQE, UIQM, PSNR, and IS metrics. We present the results obtained with *UW-CVGAN*, Deep Ssr [14], Funie gan [9], Ugan and Ugan-p [11] computed over the EuVP dataset. The last two columns present the memory space required to store the underwater image or its latent features.

model	UCIQE $\uparrow$	UIQM $\uparrow$	PSNR $\uparrow$	IS $\uparrow$	Params	Bytes
<b>UW-CVGAN (OUR)</b>	<b>6.47</b>	<b>2.91</b>	<b>29.11</b>	<b>4.39 <math>\pm</math> 0.5</b>	256 $\times$ 16 $\times$ 16	<b>262KB</b>
Deep Ssr	5.86	2.69	29.39	4.99 $\pm$ 0.7	116 $\times$ 72 $\times$ 32	1.1MB
Funie gan	6.66	2.07	29.41	5.25 $\pm$ 0.8	256 $\times$ 256 $\times$ 3	786KB
Ugan	6.00	2.15	29.34	5.24 $\pm$ 0.7	256 $\times$ 256 $\times$ 3	786KB
Ugan-p	6.30	2.12	29.31	5.08 $\pm$ 0.7	256 $\times$ 256 $\times$ 3	786KB

We demonstrate, that *UW-CVGAN* is able to reach metrics results on par with the other methods while requiring less memory storage per image by storing only the encoded image when the encoder is embedded onto the collector.

Finally, we use the Canny edge detector [45], which provides a colour agnostic evaluation of the images compared to ground truth. In Fig. 10, we show the edges detected images obtained with *UW-CVGAN* compared to the ones obtained with the other methods. We observe that the edges obtained with our methods appear to be less noisy than the other methods and visibly close to the edges in the ground truth. In Tab. 3, we consider the Euclidean distance computed between the edges detected in the input image, the edges detected in images reconstructed with each model considered for comparison. We observe that the edges obtained with *UW-CVGAN* has a lower distance from edges of the ground truth compared to the other methods. This demonstrates that the enhanced images provided by *UW-CVGAN* outperform them in the definition of details.



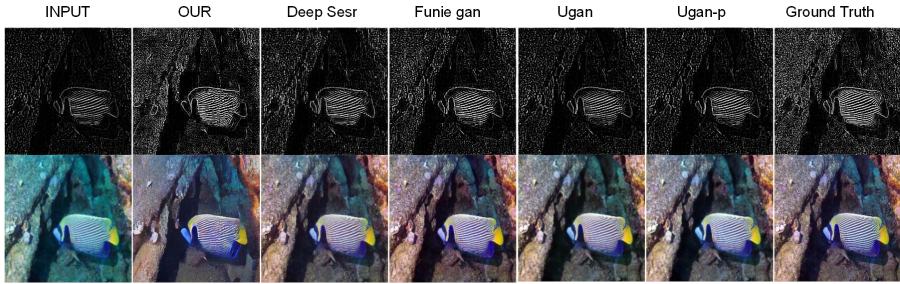


**Fig. 10** Focus of reconstruction quality of images: running the Canny Edge Detector on sample images. The first row shows the edges identified by the canny edge detector over the reconstructed images obtained with the underwater input, UW-CVGAN, and models at the state of the art Deep Ssr [14], Funie gan [9], Ugan and Ugan-p [11]. Last column is the ground truth denoised images.

**Table 3** Results Comparison Euclidean distance of Canny Edge: We summarise the Euclidean distance computed between the edges detected in original input, the edges detected in images obtained with UW-CVGAN compared with results obtained with UW-CVGAN, Deep Ssr [14], Funie gan [9], Ugan and Ugan-p [11] computed over the EuVP dataset. The results presented are to be considered multiplied to  $10E5$ .

	UW-CVGAN (OUR)	Deep Ssr	Funie gan	Ugan	Ugan-p
L2Norm	<b>344.36</b>	349.89	358.89	352.58	353.35

## 5 Discussion

The results presented in Sec. 4.5 demonstrate the ability of UW-CVGAN in image enhancement of an underwater image. In contrast with Funie gan [9], Ugan, and Ugan-p [11], UW-CVGAN reconstructs the images only from the latent space keeping the encoder and decoder networks separated. This characteristic allow to use the encoder to compress the image while collecting. In contrast with Deep Ssr [14], UW-CVGAN compresses the input image in the latent representation by a factor of 3, while Deep Ssr compress the features by a factor of 1.5. The UW-CVGAN faces a challenging reconstruction of underwater images learning to extract the latent representation of the image which is used to provide the enhanced image.

Finally, we think it is interesting to observe the model's failures. In Fig. 11, we present samples that are wrongly reconstructed. The reconstructed images appear to be desaturated, and the colourisation is brownish or greenish. This result is obtained with UW-CVGAN as with works at SOTA and highlights an interesting limit of these generative methods in colours reconstruction in underwater images. This problem is evident mainly with the input images where the red components are suppressed due to the light absorption in the water and opens up to the need of further study with such types of models.

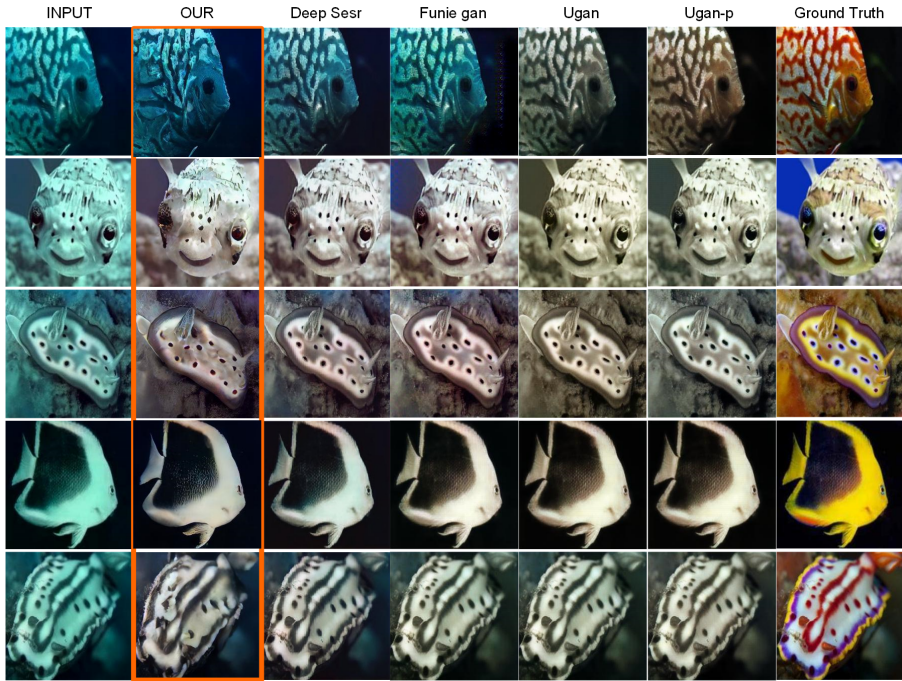


**Fig. 11** A sample of failure in images reconstruction with UW-CVGAN compared with SOTA: the first column is the input images provided to the models from EUVP dataset. We compare our results, with results obtained with models at the state of the art Deep Ssr [14], Funie gan [9], Ugan and Ugan-p [11]. Last column is the ground truth denoised images.

## 6 Conclusion

In this paper, we demonstrate the application of the capsules layer as a quantization layer for VAE by proposing CV-GAN. The new architecture is a valid tradeoff between a fully differentiable model and discrete latent features, with the compromise of dynamic learned of quantization. We propose this model for underwater image enhancement, and we train the model to reconstruct while enhancing the distorted images. We obtain results on par with SOTA on UCIQE, UIQM, PSNR, and IS metrics. Moreover, our model is an AutoEncoder where the encoder network is completely independent of the decoder. This brings up two observations: the model is able to extract representative features that are left behind the noise of the water with the only features extracted by the encoder. That proves that the encoder can be used as compressing algorithm to reduce the input image to its fundamental features obtaining  $3\times$  of compression factor. The model is the first attempt at a generative variational AutoEncoder where the capsules layer is used to perform the quantization of the latent space, and the first attempt of such a model for the underwater image enhancement. The results obtained show up high quality in reconstruction and bright and saturated colours. We finally analyse failures in image reconstruction that open up to other new challenges.

## References

- [1] Shkurti, F., Xu, A., Meghjani, M., Higuera, J.C.G., Girdhar, Y., Giguere, P., Dey, B.B., Li, J., Kalmbach, A., Prahacs, C., *et al.*: Multi-domain monitoring of marine environments using a heterogeneous robot team. In: *IROS*, pp. 1747–1753 (2012). <https://doi.org/10.1109/IROS.2012.6385685>
- [2] Whitcomb, L., Yoerger, D.R., Singh, H., Howland, J.: Advances in underwater robot vehicles for deep ocean exploration: Navigation, control, and survey operations. In: *Robotics Research*, pp. 439–448 (2000). [https://doi.org/10.1007/978-1-4471-0765-1\\_53](https://doi.org/10.1007/978-1-4471-0765-1_53)
- [3] Bingham, B., Foley, B., Singh, H., Camilli, R., Delaporta, K., Eustice, R., Mallios, A., Mindell, D., Roman, C., Sakellariou, D.: Robotic tools for deep water archaeology: Surveying an ancient shipwreck with an autonomous underwater vehicle. *Journal of Field Robotics* **27**(6), 702–717 (2010). <https://doi.org/10.1002/rob.20350>
- [4] Li, C.-Y., Guo, J.-C., Cong, R.-M., Pang, Y.-W., Wang, B.: Underwater image enhancement by dehazing with minimum information loss and histogram distribution prior. *IEEE Transactions on Image Processing* **25**(12), 5664–5677 (2016). <https://doi.org/10.1109/TIP.2016.2612882>
- [5] Ghani, A.S.A., Isa, N.A.M.: Underwater image quality enhancement through integrated color model with rayleigh distribution. *Applied soft computing* **27**, 219–230 (2015). <https://doi.org/10.1016/j.asoc.2014.11.020>
- [6] Han, P., Liu, F., Yang, K., Ma, J., Li, J., Shao, X.: Active underwater descattering and image recovery. *Applied Optics* **56**(23), 6631–6638 (2017). <https://doi.org/10.1364/AO.56.006631>
- [7] Neumann, L., Garcia, R., Jánosik, J., Gracías, N.: Fast underwater color correction using integral images. *Instrumentation Viewpoint* (20), 53–54 (2018)
- [8] Hu, K., Zhang, Y., Weng, C., Wang, P., Deng, Z., Liu, Y.: An underwater image enhancement algorithm based on generative adversarial network and natural image quality evaluation index. *Journal of Marine Science and Engineering* **9**(7), 691 (2021). <https://doi.org/10.3390/jmse9070691>
- [9] Islam, M.J., Xia, Y., Sattar, J.: Fast underwater image enhancement for improved visual perception. *IEEE Robotics and Automation Letters* **5**(2), 3227–3234 (2020). <https://doi.org/10.1109/LRA.2020.2974710>

- [10] Park, J., Han, D.K., Ko, H.: Adaptive weighted multi-discriminator cycle-gan for underwater image enhancement. *Journal of Marine Science and Engineering* **7**(7), 200 (2019). <https://doi.org/10.3390/jmse7070200>
- [11] Fabbri, C., Islam, M.J., Sattar, J.: Enhancing underwater imagery using generative adversarial networks. In: *ICRA*, pp. 7159–7165 (2018). <https://doi.org/10.1109/ICRA.2018.8460552>
- [12] Zhang, H., Sun, L., Wu, L., Gu, K.: Dugan: An effective framework for underwater image enhancement. *IET Image Processing* **15**(9), 2010–2019 (2021). <https://doi.org/10.1049/ipr2.12172>
- [13] Zhu, J.-Y., Park, T., Isola, P., Efros, A.A.: Unpaired image-to-image translation using cycle-consistent adversarial networks. In: *Proceedings of ICCV*, pp. 2223–2232 (2017)
- [14] Islam, M.J., Luo, P., Sattar, J.: Simultaneous enhancement and super-resolution of underwater imagery for improved visual perception. *arXiv:2002.01155* (2020). <https://doi.org/10.48550/arXiv.2002.01155>
- [15] Guo, Y., Li, H., Zhuang, P.: Underwater image enhancement using a multiscale dense generative adversarial network. *IEEE Journal of Oceanic Engineering* **45**(3), 862–870 (2019). <https://doi.org/10.1109/JOE.2019.2911447>
- [16] Goodfellow, I., Pouget-Abadie, J., Mirza, M., Xu, B., Warde-Farley, D., Ozair, S., Courville, A., Bengio, Y.: Generative adversarial networks. *Advances in neural information processing systems* **27** (2014)
- [17] Yuille, A.L., Liu, C.: Deep nets: What have they ever done for vision? *International Journal of Computer Vision* **129**(3), 781–802 (2021)
- [18] Oord, A.v.d., Vinyals, O., Kavukcuoglu, K.: Neural discrete representation learning. *arXiv:1711.00937* (2017)
- [19] Tjandra, A., Sisman, B., Zhang, M., Sakti, S., Li, H., Nakamura, S.: Vqvae unsupervised unit discovery and multi-scale code2spec inverter for zerospeech challenge 2019. *arXiv:1905.11449* (2019). <https://doi.org/10.48550/arXiv.1905.11449>
- [20] Eloff, R., Nortje, A., van Niekerk, B., Govender, A., Nortje, L., Pretorius, A., Van Biljon, E., van der Westhuizen, E., van Staden, L., Kamper, H.: Unsupervised acoustic unit discovery for speech synthesis using discrete latent-variable neural networks. *arXiv:1904.07556* (2019). <https://doi.org/10.48550/arXiv.1904.07556>

- [21] Jang, E., Gu, S., Poole, B.: Categorical reparameterization with gumbel-softmax. *arXiv:1611.01144* (2016). <https://doi.org/10.48550/arXiv.1611.01144>
- [22] Łańcucki, A., Chorowski, J., Sanchez, G., Marxer, R., Chen, N., Dolfing, H.J., Khurana, S., Alumäe, T., Laurent, A.: Robust training of vector quantized bottleneck models. In: *International Joint Conference on Neural Networks (IJCNN)*, pp. 1–7 (2020). <https://doi.org/10.1109/IJCNN48605.2020.9207145>
- [23] Esser, P., Rombach, R., Ommer, B.: Taming transformers for high-resolution image synthesis. In: *Proceedings of CVPR*, pp. 12873–12883 (2021)
- [24] Sabour, S., Frosst, N., Hinton, G.E.: Dynamic routing between capsules. In: *Advances in Neural Information Processing Systems*, pp. 3856–3866 (2017)
- [25] Pucci, R., Micheloni, C., Foresti, G.L., Martinel, N.: Fixed simplex coordinates for angular margin loss in capsnet. In: *25th ICPR*, pp. 3042–3049 (2021)
- [26] Pucci, R., Micheloni, C., Foresti, G.L., Martinel, N.: Deep interactive encoding with capsule networks for image classification. *Multimedia Tools and Applications* **79**(43), 32243–32258 (2020)
- [27] Deng, F., Pu, S., Chen, X., Shi, Y., Yuan, T., Pu, S.: Hyperspectral image classification with capsule network using limited training samples. *Sensors* **18**(9), 3153 (2018). <https://doi.org/10.3390/s18093153>
- [28] Pucci, R., Micheloni, C., Martinel, N.: Collaborative image and object level features for image colourisation. In: *Proceedings of CVPR*, pp. 2160–2169 (2021)
- [29] Pucci, R., Micheloni, C., Foresti, G.L., Martinel, N.: Pro-ccaps: Progressively teaching colourisation to capsules. In: *Proceedings of WACV*, pp. 2271–2279 (2022)
- [30] Mello, C.D., Moreira, B.U., Drews, P.L., Botelho, S.C.: Alternative underwater image restoration based on unsupervised learning and autoencoder with degradation block. In: *LARS*, pp. 1–6 (2020). <https://doi.org/10.1109/LARS/SBR/WRE51543.2020.9307136>
- [31] Kingma, D.P., Welling, M.: Auto-encoding variational bayes. *arXiv:1312.6114* (2013). <https://doi.org/10.48550/arXiv.1312.6114>
- [32] Jaffe, J.S.: Computer modeling and the design of optimal underwater

- imaging systems. *IEEE Journal of Oceanic Engineering* **15**(2), 101–111 (1990). <https://doi.org/10.1109/48.50695>
- [33] McGlamery, B.: Computer analysis and simulation of underwater camera system performance. *SIO ref* **75**(2) (1975)
- [34] Isola, P., Zhu, J.-Y., Zhou, T., Efros, A.A.: Image-to-image translation with conditional adversarial networks. In: *Proceedings of CVPR*, pp. 1125–1134 (2017)
- [35] Zhang, R., Isola, P., Efros, A.A., Shechtman, E., Wang, O.: The unreasonable effectiveness of deep features as a perceptual metric. In: *Proceedings of CVPR*, pp. 586–595 (2018). <https://doi.org/10.1109/cvpr.2018.00068>
- [36] Mathieu, M., Couprie, C., LeCun, Y.: Deep multi-scale video prediction beyond mean square error. *arXiv:1511.05440* (2015). <https://doi.org/10.48550/arXiv.1511.05440>
- [37] Russakovsky, O., Deng, J., Su, H., Krause, J., Satheesh, S., Ma, S., Huang, Z., Karpathy, A., Khosla, A., Bernstein, M., *et al.*: Imagenet large scale visual recognition challenge. *International journal of computer vision* **115**(3), 211–252 (2015). <https://doi.org/10.1007/s11263-015-0816-y>
- [38] Han, J., Shoeiby, M., Malthus, T., Botha, H., Anstee, J., Wei, R., Petersson, L., Armin, A.: Heron Island Coral Reef Dataset. v2. CSIRO. Data Collection. (2021)
- [39] Peng, L., Zhu, C., Bian, L.: U-shape Transformer for Underwater Image Enhancement (2021). <https://doi.org/10.48550/arXiv.2111.11843>
- [40] Salimans, T., Goodfellow, I., Zaremba, W., Cheung, V., Radford, A., Chen, X.: Improved techniques for training gans. *Advances in neural information processing systems* **29** (2016)
- [41] Hore, A., Ziou, D.: Image quality metrics: Psnr vs. ssim. In: *20th ICPR*, pp. 2366–2369 (2010). <https://doi.org/10.1109/ICPR.2010.579>
- [42] Yang, M., Sowmya, A.: An underwater color image quality evaluation metric. *IEEE Transactions on Image Processing* **24**(12), 6062–6071 (2015). <https://doi.org/10.1109/TIP.2015.2491020>
- [43] Panetta, K., Gao, C., Agaian, S.: Human-visual-system-inspired underwater image quality measures. *IEEE Journal of Oceanic Engineering* **41**(3), 541–551 (2016). <https://doi.org/10.1109/JOE.2015.2469915>
- [44] Obukhov, A., Seitzer, M., Wu, P.-W., Zhydenko, S., Kyl, J., Lin, E.Y.-J.: High-fidelity performance metrics for generative models in PyTorch.

*Zenodo* (2020). <https://doi.org/10.5281/zenodo.4957738>

- [45] Canny, J.: A computational approach to edge detection. *Transactions on PAMI* (6), 679–698 (1986). <https://doi.org/10.1016/b978-0-08-051581-6.50024-6>